

Collective Dynamics of Josephson Vortices in Intrinsic Josephson Junctions: Exploration of In-phase Locked Superradiant Vortex Flow States

^a M. Machida

*Center for Promotion of Computational Science and Engineering,
Japan Atomic Energy Research Institute, 2-2-54 Nakameguro, Meguro-ku Tokyo 153, Japan*
^a CREST, Japan Science and Technology Corporation(JST), Japan

T.Koyama

Institute for Materials Research, Tohoku University, Katahira 2-1-1, Aoba-ku, Sendai 980-77, Japan

A.Tanaka

Teikyo University of Science, Uenohara 2525, Yamanashi, Japan

M.Tachiki

National Research Institute for Metals, Sengen 1-2-1, Tsukuba, Ibaraki 305, Japan
(October 13, 2018)

In order to clarify the “superradiant” conditions for the moving Josephson vortices to excite in-phase AC electromagnetic fields over all junctions, we perform large scale simulations of realistic dimensions for intrinsic Josephson junctions under the layer parallel magnetic field. Three clear step-like structures in the I-V curve are observed above a certain high field ($H > 1T$ in the present simulations), at which we find structural transitions in the moving flux-line lattice. The Josephson vortex flow states are accordingly classified into four regions (region I \sim IV with increasing current), in each of which the power spectrum for the electric field oscillations at the sample edge are measured and typical snapshots for Josephson vortex configurations are displayed. Among the four regions, especially in the region III, an in-phase rectangular vortex lattice flow state emerges and the power spectrum shows remarkably sharp peak structure, i.e., superradiant state. Comparison of the simulation results with an eigenmode analysis for the transverse propagating Josephson plasma oscillations reveals that the resonances between Josephson vortex flow states and some of the eigenmodes are responsible for the clear flux lattice structural transitions. Furthermore, the theoretical analysis clarifies that the width of the superradiant state region in the I-V characteristics enlarges with decreasing both the superconducting and insulating layer thickness.

PACS numbers: 74.50.+r, 74.60.Ge, 74.80.Dm, 85.25.Cp

I. INTRODUCTION

Intrinsic Josephson effects (IJE's) in highly anisotropic high temperature superconductors (HTSC's) such as $\text{Bi}_2\text{Sr}_2\text{CaCu}_2\text{O}_8$ is a subject currently under intensive investigation [1]. This is because single crystals of these materials naturally form a stack of many atomic-scale Josephson junctions, i.e., intrinsic Josephson junctions (IJJ's) and therefore strong coherence between junctions are expected. Especially, if in-phase oscillation over all junctions is realized it will show superradiant properties such as remarkable increase of output power and decrease of linewidth [2-7], and its realization will give a great impact on technological applications to optical communications in the near future. Therefore, in this paper, we explore such superradiant conditions in Josephson vortex flow states in IJJ's.

In the case of the single long Josephson junctions (SLJJ's), fluxon dynamics coupled with transverse prop-

agating Josephson plasma oscillation have already been extensively investigated [8], [9], [10], and SLJJ's have been employed as useful flux flow oscillators. In SLJJ's, the fluxons are aligned like one-dimensional chain along the junction plane and unidirectionally driven under the bias-current. This sliding motion of the fluxon chain excites the transverse propagating Josephson plasma oscillations inside the junction, and when their moving speed matches the Josephson plasma mode velocity, I-V characteristics show a step like resonant structure, where the electromagnetic (EM) wave radiation power becomes maximal [10], [11].

On the other hand, IJJ's have a longitudinal propagating Josephson plasma mode along the stacked direction and its dispersion relation are shown to be very different from that of the transverse mode, i.e., the longitudinal one is almost flat while the transverse one is very dispersive. Thus, IJJ's can have many propagating modes with different dispersions as mixtures between transverse and

longitudinal modes, and IJJ systems with finite stacking height (employed in experiments) have the standing waves for those mixed modes along the stacked direction [2], [3]. Accordingly, the I-V characteristics and the properties of EM radiation in IJJ's are clearly expected to exhibit a rich variety in contrast to SLJJ's. Actually, so far, the fluxon dynamics in IJJ's have been investigated in several papers[2-7], [12] to understand their dynamics and related EM radiation, and complex resonant behaviors with some special modes have been reported. However, the full understanding for the behavior of the fluxons and Josephson plasma oscillations has not been achieved. Especially, the clear in-phase superradiant conditions in IJJ's have not yet been established, and some questions still now remain concerning the stability of the superradiant flow state and its emergent region with respect to experimental variables as the magnetic field and the transport current. Therefore, in this paper, we report results of the first direct large scale simulations for the fluxon dynamics in IJJ's using the coupled Sine-Gordon equation and clarify the superradiant conditions. Furthermore, we pay attention to all dynamical flux flow states observed in various current ranges in the I-V characteristics and reveal that the I-V characteristics show three clear step-like structures corresponding to flux lattice structural transitions. Thus, we distinguish flux flow states into four regions at these three step-like structures, and display the typical flux flow lattice configuration in each of the regions. The names region I ~ IV (in increasing order of the current) will be assigned to the four regions. In order to identify the natures of the EM radiations in the four regions, the electric field oscillations at the sample edge, which characterize the properties of the emitted electromagnetic wave, are measured and their typical power spectrum in each region is given.

Here, let us briefly describe the characters of the flux flow states observed in the four regions. The notable points are remarkable differences in the flux lattice configurations and power spectra for EM field oscillations in those four regions. In region I, fluxons flow randomly without forming a clear lattice structure. This state is a steady state when the applied current is low enough, and the electric field oscillations at the edge exhibit a broad-band power spectrum. In region II, wavy aligned flux flow states appear. From this region, the vortex flow states begin to show resonances with some of the transverse propagating modes. The vortex alignments develop along the stacked direction, and the power spectrum has peak structures at a characteristic frequency and its higher harmonics. In region III, a perfect in-phase flux flow states emerges. The vortex alignment becomes perfect along the c-axis and fluxons form a rectangular lattice. The line-width of the power spectrum is very sharp and the power at the peak position is also very large, i.e., the superradiant state. In region IV, triangular like lattice flux flow states are observed. Its Josephson frequencies due to the flux flow voltages are larger than the frequencies of any plasma modes. Conse-

quently, it is expected that the transverse plasma modes does not affect the formation of flux lattice structures and therefore energetic favorable triangular like lattice flow states appear. In order to understand the origin of the transitions between these four flux flow states, we perform an eigenmode analysis on the employed coupled Sine-Gordon equation. As a result, we are able to identify that the resonances between three modes and the flux flow states leads to three clear step-like structures in the I-V characteristics. Thus, from this theoretical analysis, we can predict the width of the four regions, especially, the superradiant state (region III), in the I-V characteristics. Also, the analysis clarifies that the superradiant state region enlarges with increasing a parameter ratio, $\frac{\lambda_{ab}^2}{sD}$, where s and D are, respectively, superconducting and insulating layer thickness and λ_{ab} is the penetration depth in the ab-plane direction. This result clearly indicates that IJJ's can have remarkably wide superradiant region in I-V characteristics.

The outline of this paper is as follows. The model equation employed is briefly introduced in section II, and the numerical simulation results are shown in section III. Section IV is devoted to eigen mode analysis and discussions.

II. MODEL EQUATION

We first explain our model. We perform the simulations under a configuration in which the transport current flows in the direction perpendicular to the junctions (\parallel z-axis) and the magnetic field is applied along the junctions (\parallel y-axis) as shown in Fig.1.

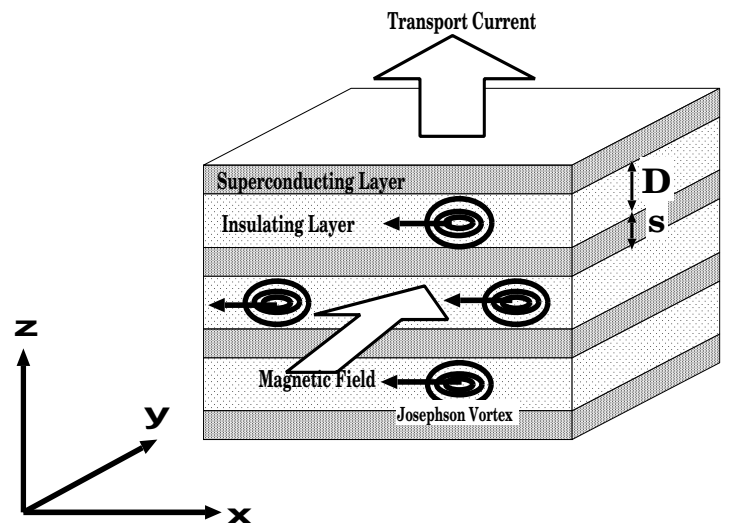


FIG.1 A schetch of the intrinsic Josephson junction. The magnetic field and the transport current are applied along the junction plane (y-axis) and the stacked directions (z-axis), respectively. The Josephson vortices move in the -x direction.

The Josephson vortices move parallel to the $-x$ -axis in this configuration. Assuming that the superconducting layers have an atomic-scale thickness, we neglect the variation of physical quantities along the z -axis inside the superconducting layers. Then, the vector potential is defined only inside the insulating layers as $A_{\ell+1,\ell}^z(x,t) (\equiv \int_{\ell}^{\ell+1} dz A_z(x,t))$, where ℓ stands for the layer index, and the electromagnetic fields $E_{\ell+1,\ell}^z(x,t)$ and $B_{\ell+1,\ell}^y(x,t)$ are, respectively given by $E_{\ell+1,\ell}^z(x,t) = -\frac{1}{cD} \frac{\partial A_{\ell+1,\ell}^z}{\partial t} - \frac{\varphi_{\ell+1} - \varphi_{\ell}}{D}$, and $B_{\ell+1,\ell}^y(x,t) = \frac{A_{\ell+1,\ell}^x - A_{\ell}^x}{D} - \frac{1}{D} \frac{\partial A_{\ell+1,\ell}^z}{\partial x}$. We assume Maxwell's equations in the present system as follows,

$$\frac{\partial B_{\ell+1,\ell}^y}{\partial x} = \frac{4\pi}{c} j_{\ell+1,\ell}^z + \frac{\epsilon_c}{c} \frac{\partial E_{\ell+1,\ell}^z}{\partial t}, \quad (1)$$

$$E_{\ell+1,\ell}^z - E_{\ell,\ell-1}^z = \frac{4\pi s}{\epsilon_c} \rho_{\ell}, \quad (2)$$

where ρ_{ℓ} and ϵ_c are, respectively, the charge density at ℓ -th superconducting layer and the dielectric constant of the insulating layers. The current, $j_{\ell+1,\ell}^z$ in eq.(1) is given by a sum of Josephson and quasiparticle currents as $j_c \sin P_{\ell+1,\ell} + \sigma E_{\ell+1,\ell}^z$, with j_c and σ being the critical current density and conductivity of the quasiparticles, respectively. $P_{\ell+1,\ell}$ is the gauge invariant phase difference defined as $P_{\ell+1,\ell} = \theta_{\ell+1} - \theta_{\ell} - \frac{2\pi}{\phi_0} A_{\ell+1,\ell}$ with θ_{ℓ} being the phase of the superconducting order parameter of ℓ -th layer. The time and spatial derivatives for $P_{\ell+1,\ell}$ yield the generalized relations,

$$\frac{\partial P_{\ell+1,\ell}}{\partial t} = -4\pi\mu^2 \frac{2\pi c}{\phi_0} (\rho_{\ell+1} - \rho_{\ell}) + \frac{2\pi c D}{\phi_0} E_{\ell+1,\ell}^z, \quad (3)$$

$$\frac{\partial P_{\ell+1,\ell}}{\partial x} = \frac{4\pi\lambda_{ab}^2}{c} \frac{2\pi}{\phi_0} (j_{\ell+1}^x - j_{\ell}^x) + \frac{2\pi D}{\phi_0} B_{\ell+1,\ell}^y, \quad (4)$$

where λ_{ab} are the penetration depth associated with the current j_{ℓ}^x in the ab -plane and μ is the Debye length [13] [14]. In deriving eq.(3) and (4), we employ the equation $\rho_{\ell} = -\frac{1}{4\pi\mu^2} (\frac{\phi_0}{2\pi c} \partial_t \theta_{\ell} + \varphi_{\ell})$, which is analogous to the London equation and the London equation for the in-plane current, $j_{\ell}^x = -\frac{c}{4\pi\lambda_{ab}^2} (\frac{\phi_0}{2\pi} \nabla_x \theta_{\ell} - A_{\ell}^x)$. In the case where $j_{\ell+1}^x - j_{\ell}^x \neq 0$ under an external magnetic field the first term on the right hand side of eq.(3) gives only small contribution of $O(\mu^2/\lambda_{ab}^2)$ to the dynamics of $P_{\ell+1,\ell}$, which means that the incomplete screening effect for charges in the superconducting layers, namely the coupling between junctions due to the charge neutrality breaking effect [13], [14] may be neglected in the presence of an external magnetic field. Then, in this approximation the equation for $P_{\ell+1,\ell}$ is derived from eqs.(1)-(4) as follows [13], [15], [16]

$$\begin{aligned} \frac{\partial^2 P_{\ell+1,\ell}}{\partial t'^2} &= \frac{\lambda_{ab}^2}{sD} \left(\frac{\partial^2 P_{\ell+2,\ell+1}}{\partial t'^2} + \frac{\partial^2 P_{\ell,\ell-1}}{\partial t'^2} - 2 \frac{\partial^2 P_{\ell+1,\ell}}{\partial t'^2} \right) \\ &+ \frac{\lambda_{ab}^2}{sD} (\sin P_{\ell+2,\ell+1} + \sin P_{\ell,\ell-1} - 2 \sin P_{\ell+1,\ell}) \\ &+ \beta \frac{\lambda_{ab}^2}{sD} \left(\frac{\partial P_{\ell+2,\ell+1}}{\partial t'} + \frac{\partial P_{\ell,\ell-1}}{\partial t'} - 2 \frac{\partial P_{\ell+1,\ell}}{\partial t'} \right) \end{aligned}$$

$$+ \frac{\partial^2 P_{\ell+1,\ell}}{\partial x'^2} - \sin P_{\ell+1,\ell} - \beta \frac{\partial P_{\ell+1,\ell}}{\partial t'}, \quad (5)$$

where $t' = \omega_p t$ and $x' = \lambda_c x$ with ω_p and λ_c being, respectively, the Josephson plasma frequency ($\omega_p = \frac{c}{\sqrt{\epsilon}\lambda_c}$) and the penetration depth in the c -axis direction. The parameter $\beta (\equiv \frac{4\pi\sigma\lambda_c}{\sqrt{\epsilon}c})$ is related the McCumber parameter β_c as $\beta_c = 1/\beta^2$. It is noted that eq.(5) gives a flat dispersion relation for the longitudinal mode along the c -axis while it leads to the dispersive one along the junctions.

III. RESULTS OF NUMERICAL EXPERIMENTS AND DISCUSSIONS

In this paper, we numerically solve eq.(5) for a finite size IJJ composed of 20 junctions in which the ac cross section (the xy -plane in Fig.1) has 2-dimensional (2D) rectangular shape in the presence of an applied field ($\parallel y$ -axis) and a transport current ($\parallel z$ -axis). The transport current and the magnetic field which includes the self-field are introduced through the boundary conditions at the top and bottom layers and the edges of all the layers. To perform the simulations we divide the system into 400 meshes along the x -direction. Each mesh is assumed to be $0.1\lambda_{ab}$ wide along the x -direction. Then the system used in the simulations has the area of $10\mu m \times 20$ junctions if we assume $\lambda_c = 125\mu m$ and $\gamma = 500$ for the anisotropic parameter, which are typical parameter values in $\text{Bi}_2\text{Sr}_2\text{CaCu}_2\text{O}_8$. The value of the material parameter β is chosen as $\beta = 0.1 (\beta_c = 100)$, which is also a typical value in $\text{Bi}_2\text{Sr}_2\text{CaCu}_2\text{O}_8$. The results shown in this paper are qualitatively size-independent. We confirmed this by performing the simulations for system sizes up to $30\mu m \times 80$ junctions in real scale.

Let us now present the results of numerical simulations. The applied magnetic field used in the following calculations is fixed to a value, $2T$. The results for lower fields ($< 1T$), which are qualitatively different, will be published elsewhere. Figure 2(a) shows the $I - V$ characteristics of IJJ. As seen in this figure, three clear steps appear at the voltage values indicated by arrows in the $I - V$ curve. To understand the origin of the steps, we plot the time and spatial averages of the Poynting vector, $\langle P_{-x} \rangle = \langle \frac{c}{4\pi S} \int dx \sum_{\ell} E_{\ell+1,\ell}^x B_{\ell+1,\ell}^y \rangle$, and the Josephson current, $\langle J_z \rangle = \langle \frac{1}{S} \int dx \sum_{\ell} \sin P_{\ell+1,\ell} \rangle$ in Fig.2 (b) and (c), where $\langle \rangle$ stands for the time average and S is the area of the computational region. Note that $\langle P_{-x} \rangle$ represents the energy flow of the transverse EM field and $\langle J_z \rangle$ gives a measure of the viscosity against the driven flux-flow. It is seen that the anomalous structures also appear in these averages, i.e., the step-like structure in $\langle P_{-x} \rangle$ and the peaks in $\langle J_z \rangle$, at the same voltage values as in the $I - V$ characteristics. Such anomalies are commonly observed in our simulations in

the case where the magnetic field is greater than 1T. Thus, it is found that the vortex dynamics are directly coupled with the transverse EM field and the vortex viscosity drastically changes at the step like structures. Especially, it is noted that the viscosity of the Josephson vortices takes maximum values at the steps. From this fact one may expect that the collective vortex dynamics changes at the steps. In the following, we, therefore, separate the voltage region into four from I to IV at the steps as shown in Fig.2(a) and investigate the collective properties of each flux-flow state separately.

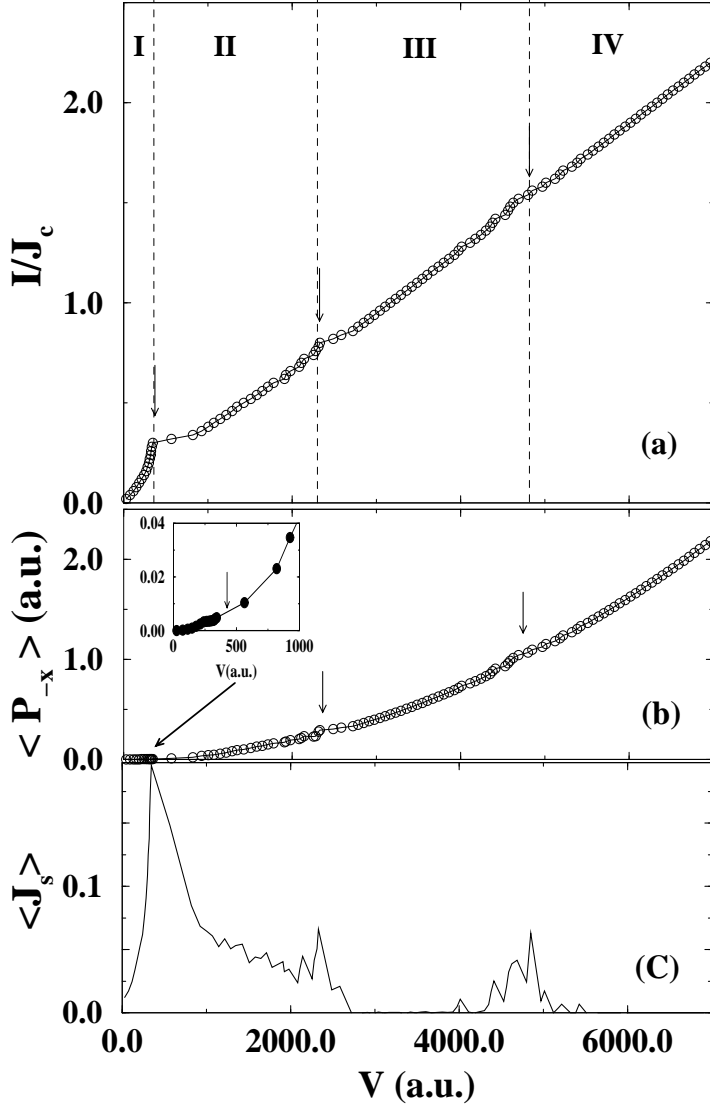


FIG.2 (a) The I-V characteristics. (b) The averaged poynting vector in x-direction $\langle P_{-x} \rangle$ vs. V . The inset of (b) gives the enlarged view of the region indicated by the inclined arrow. (c) The averaged Josephson current vs. V .

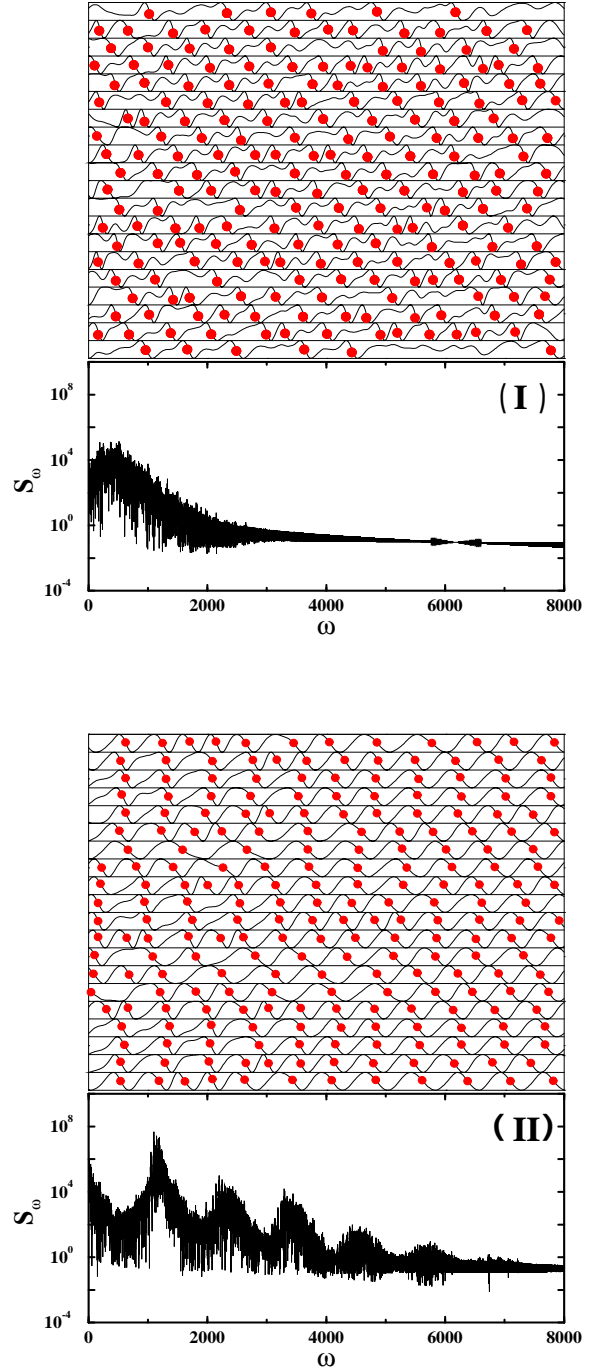


FIG.3, The snapshot of the vortex center positions along with $\sin P_{\ell+1,\ell}$ distributions in all junction sites and the power spectrum of the electric field at the left edge in the regions from I to IV: (I) $I/J_c = 0.20$, (II) $I/J_c = 0.52$. Note that the Josephson plasma frequency at the zero temperature, $\omega_p = \frac{c}{\sqrt{\epsilon_c \lambda_c(0)}}$, corresponds to $\omega = 130$ in the figures for the power spectrum.

Let us study the flux-flow state in region I first. In

Fig.3(I) we show a snapshot of the distribution of the Josephson current, $\sin P_{\ell+1,\ell}$, and the centers of the Josephson vortices (indicated by dots) together with the power spectrum of the electric field at the left edge of the sample, $S_\omega \equiv \frac{2\pi}{T} |\frac{1}{2\pi} \int_0^T \sum_\ell E_{\ell+1,\ell}(0,t) e^{i\omega t} dt|^2$. As seen in this figure, the vortices are distributed almost randomly and the power spectrum shows ω^{-2} dependence above some frequency, which indicates the irregular motion of vortices. We confirmed this chaotic behavior of moving vortices by monitoring directly the time development of the vortex positions too. From these results one may conclude that the highly viscous flux-flow state is realized in region I. The fluxons are easily pinned by any type of inhomogeneities, e.g., crystal imperfections, sample boundary etc. in this low driving-current regime. In the present system without imperfections the sample boundaries including the top and bottom junctions work as effective pinning centers, which is seen from the fact that the number of vortices in the top and bottom junctions is much smaller than that in other intermediate junctions. It is also noticed that the power spectrum forms a broad band in the low frequency region. Thus, the chaotic viscous flux motion generates a broad-band oscillating EM field in region I. The intensity of the emitted EM field increases with increasing voltage values in this region.

Let us next turn to the region II. As seen in the snapshot given in Fig.3(II), a wavy-chain-like vortex distribution is stabilized in this region. This result indicates that a correlation between vortices is developed in region II. Accordingly some characteristic frequency and its higher harmonics appear inside the broad band spectrum of the EM field. These frequencies are related to the quasi-periodicity of the moving vortex lattice. It is also noted that the frequency of the highest peak seen in the figure is about eight times larger than the Josephson plasma frequency at zero temperature, $\omega_p (= \frac{c}{\sqrt{\epsilon} \lambda_c})$. This frequency corresponds to about 4THz in the case of $\lambda_c = 125\mu m$ and $\epsilon_c = 25$.

When the voltage is further increased and reaches the value at the boundary between the regions II and III, the moving vortices form a rectangular lattice as shown in Fig.3(III). This regular distribution of the vortices is stable and maintained throughout the region III. It is seen that sharp peaks appear in the power spectrum of the EM field. The frequencies giving the peaks are determined by the flux flow velocity and the period of the lattice. Note that the phase differences of all the junctions make perfect in-phase motion in this state, that is, *the superradiant state is realized in the region III*. In this superradiant state one may expect the strong radiation of the coherent EM field from the junctions. The frequencies of the emitted EM field will be tunable in a wide range by the applied magnetic field or the voltage since the region III is broad as seen in the $I - V$ curves.

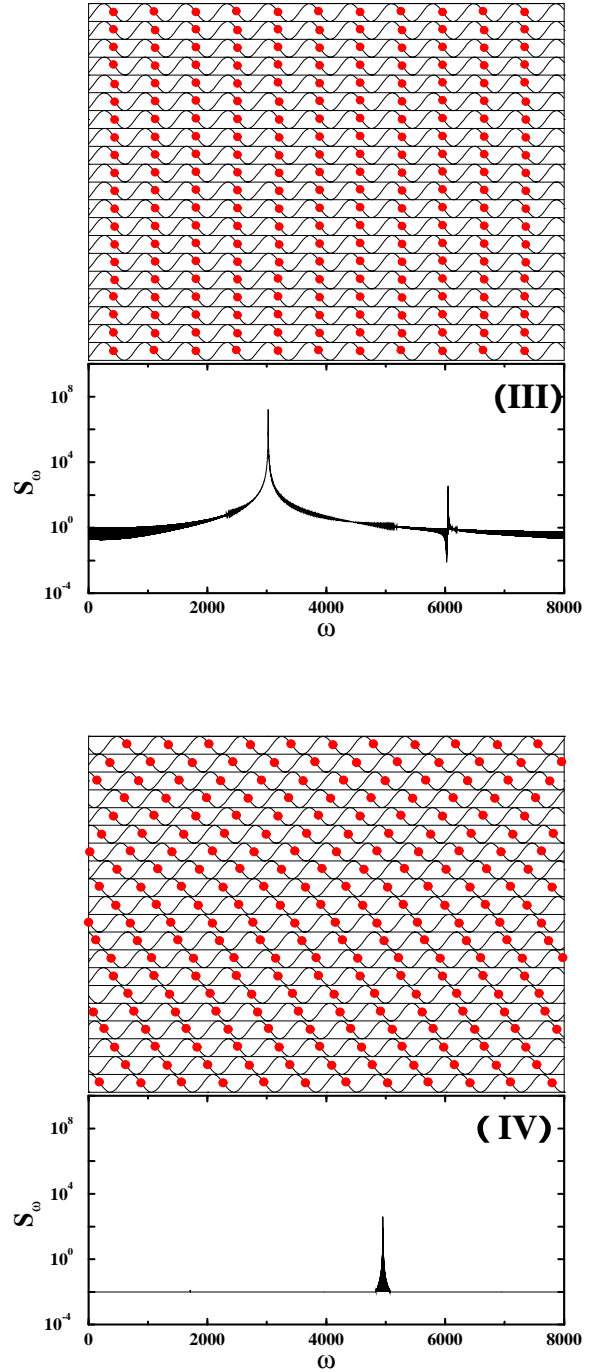


FIG.3 (III) $I/J_c = 1.16$, (IV) $I/J_c = 1.90$.

The rectangular lattice of the moving vortices becomes unstable at the boundary between the regions III and IV. The moving vortex lattice appearing in the region IV is a modulated triangular one as depicted in Fig.3(IV). The power spectrum given in Fig.3(IV) indicates that the intensity of the EM field generated in this state is greatly reduced from that in the region III. This result is

easily understood in the following way. The oscillatory components of the tunneling current on two consecutive junctions cannot be in-phase in a triangular-like lattice. As a result, the EM field generated at the junction edges on consecutive junctions interfere destructively with each other and, therefore, the intensity of the power spectrum drastically decreases in this region.

IV. EIGEN MODE ANALYSIS AND DISCUSSION

To understand the origin of the transitions in the moving vortex state we perform a linear analysis in the following. The linearized equation obtained from eq.(5) in the case of $\beta = 0$ yields the eigenvalues, $\omega_n(k_x) = \{1 + k_x^2/[1 + \frac{2\lambda_{ab}^2}{sD}(1 - \cos \frac{n\pi}{N})]\}^{1/2}$, and the eigenfunctions, $P_{\ell+1,\ell}(x', t') = e^{ik_x x'} e^{i\omega_n t'} f_{\ell+1,\ell}^{(n)}$ with $f_{\ell+1,\ell}^{(n)} = g_n e^{i\pi \ell n/N}$ for the system with N junctions, where n specifies the eigenmode, i.e., $n = 1, \dots, N-1$. These eigenmodes may be interpreted to be the transverse Josephson plasma modes in finite IJJ composed of N junctions without vortices. In the inset of Fig.4(a) we plot the spatial variation of $\text{Re}(f_{\ell+1,\ell}^{(n)})$ for four values ($n=0, 1, 2$, and 19) of n in the case of $N = 20$, which represents the standing waves along the c -axis. In the presence of an external magnetic field, H , and a DC voltage, V , eq.(5) has an approximate solution corresponding to the phase-locked flux-flow state as $P_{\ell+1,\ell}(x', t') = H'x' - V't' + h_{\ell+1,\ell}(x', t')$, where $H' = \frac{2\pi D \lambda_c}{\phi_0} H$ and $V' = \frac{2\pi c}{\phi_0 \omega_p} V$. Here, the function $h_{\ell+1,\ell}(x', t')$ is assumed to be an small oscillatory component. In this case, $h_{\ell+1,\ell}(x', t')$ satisfies approximately the equation, $[(1 - \frac{\lambda_{ab}^2}{sD} \Delta^{(2)}) \partial_t^2 - \partial_x^2] h_{\ell+1,\ell} = -\sin(H'x' - V't')$, where $\Delta^{(2)}$ is defined by $\Delta^{(2)} h_{\ell+1,\ell} = h_{\ell+2,\ell+1} + h_{\ell,\ell-1} - 2h_{\ell+1,\ell}$ [2], [8]. This equation has solutions showing resonances at $\omega \sim H'/\{1 + \frac{2\lambda_{ab}^2}{sD}(1 - \cos \frac{n\pi}{N})\}^{1/2}$. This resonant behavior originates as a result that the Josephson oscillations induced by the moving flux-line lattice match the transverse Josephson plasma frequencies. Note that the resonant frequencies coincide with the eigen-frequencies $\omega_n(k_x)$ for $k_x = H' \gg 1$. Figure 4(a) shows the matching voltages ($V' = \omega_n(k_x = H')$) as a function of H in the case of $N = 20$. In Fig.4(b), we superpose the vertical lines indicating the matching voltages at $k_x = H (= 2T)$ on the $I - V$ curve. As seen in this figure, the voltages matching with the modes A ($n = 0$) and B ($n = 1$) coincide with the 3rd and 2nd steps and the lowest matching voltage is also located close to the 1st step in the $I - V$ curves. These analyses indicate that the structural transitions in the moving flux-line lattice are caused by the matching of the phase oscillations arising from the vortex motion with that of the eigen-modes of the system.

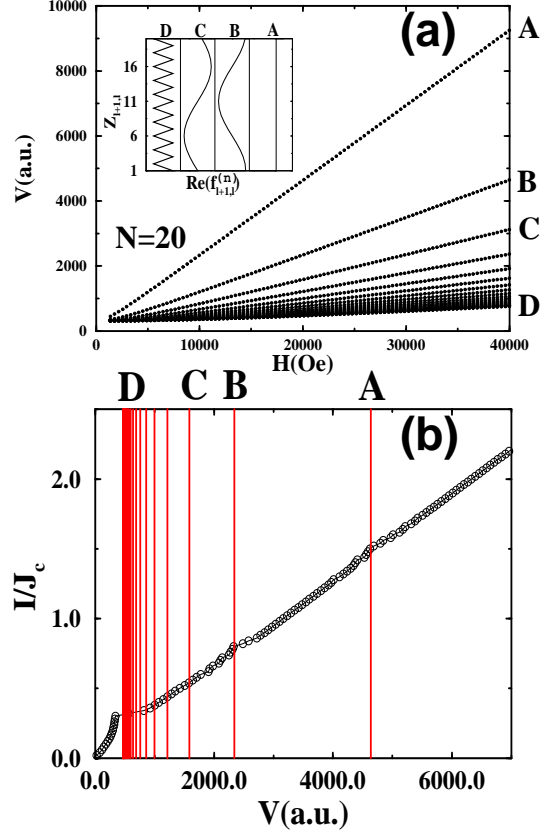


FIG.4, (a) The magnetic field dependence of the matching voltage between the flux flow states and all transverse eigenmodes. The inset shows the variations along c -axis of $\text{Re}(f_{\ell+1,\ell}^{(n)})$ of A($n = 0$), B($n = 1$), C($n = 2$) and D($n = 19$) modes, where $f_{\ell+1,\ell}^{(n)} = g_n e^{i\pi \ell n/N}$. (b) The $I - V$ characteristics same as Fig.1(a). The vertical lines indicate the matching voltage of all eigenmodes, and A, B, C, and D correspond to those shown in Fig.4(a), respectively

Here, it is noted that not all the matching voltages cause clear step-like anomalies in the $I - V$ characteristics. However, we have directly observed the structural change, for example, near the voltage value at C by monitoring the vortex configuration. Since the $I - V$ characteristics is given by a sum of the contribution from all the junctions, it is understood that it is not so sensitive for a slight structural change in the moving flux-line lattice, that is, in a case that the current distribution is not largely altered at the transition, a clear anomalous structure will not appear in the $I - V$ characteristics. We also notice that the matching with the modes, A and B, obtained in the above linear analyses gives the precise phase boundaries of the region III. This fact indicates that the above analysis is sufficiently valid in this region, that is, the oscillatory part $h_{\ell+1,\ell}$ is only a small perturbation and the phase-locked in-phase flux-flow state, which is the moving rectangular-lattice

state, is very stable. The width of the region III is given by $\Delta V = \omega_A(H) - \omega_B(H) \sim [1 - \frac{\sqrt{sD}}{\sqrt{2}\lambda_{ab}} \frac{1}{\sqrt{1-\cos(\pi/N)}}]H$.

Since $\frac{\sqrt{sD}}{\sqrt{2}\lambda_{ab}}$ is very small in high- T_c superconductors, the superradiant state is expected to be very wide in IJJ's.

Hechtfisher et al. observed a broad-band emission in the flux-flow state of $\text{Bi}_2\text{Sr}_2\text{CaCu}_2\text{O}_8$ single crystals, whose power spectrum takes a maximum around the voltage at which the step-like structure appears in the $I - V$ characteristics [18]. They claim that the EM waves emitted from the junctions are generated by the Cherenkov radiation due to the moving vortices [18], [19]. From our simulation results, we may suggest two possibilities for the origin of the broad-band emission. The first one is the Cherenkov-type radiation as claimed by Hechtfisher et al. Rough estimation for the present model indicates that the threshold voltage for the Cherenkov radiation lies in region II, in which we really observe the broad-band spectrum in the low-frequency region as seen in Fig.3(II). It is noted that this result is consistent with simulation results by Hechtfisher et al [19]. In this scenario, the step-like anomaly observed in the $I - V$ curve of Bi-2212 may be identified with the boundary between the regions II and III in our simulations. On the other hand, it is also possible to interpret that the step corresponds to the boundary between the regions I and II, which leads to another possibility for the origin of the observed broad-band emission. In this second scenario, it is understood that the observed EM field originates from the vortex state in region I. Since no transverse propagating Josephson plasma mode can be coupled with such the slow vortex motions in this region, one may interpret that the broad-band spectrum reflects chaotic EM field oscillations due to the non-regular motion of vortices. Here, note that step structure in IVC at the boundary between the region I and II in simulations is the most remarkable structure and it is similar with experimental results [18]. To clarify the mechanism of the broad-band emission, we will need more detailed theoretical and experimental studies.

V. CONCLUSION

In conclusion, we performed direct large scale numerical simulations on Josephson vortex flow states in IJJ's and find structural transitions of the moving flux-line lattice accompanied by the step-like structures in the $I-V$ characteristics and changes of power spectrums of AC electric field at the sample edge. The four typical flux flow states and the corresponding power spectra are identified and the in-phase superradiant flux flow state are found to exist stably in a wide region in the $I-V$ characteristics. The comparison between the simulation results and the eigenmode analysis for the transverse propagating Josephson plasma modes show that those step-like structures in the $I-V$ characteristics are due to resonances between

flux flow motions and transverse propagating Josephson plasma modes. Furthermore, the analysis predicts that the superradiant state region enlarges as the superconducting and insulating layer thickness is decreased compared to the magnetic penetration depth in the ab -plane direction. The collective Josephson vortex flow under the presence of many propagating modes includes very rich varieties of physics, while the stable superradiant flux flow state will be a key feature in making successfully submillimeter-wave generator employing IJJ's.

The authors thank T.Yamashita, and S.Sakai for useful discussions and one of us (M.M.) also thank for T.Imamura and M.Itakura for numerical simulation techniques and K. Asai and H. Kaburaki for their supports on the computer simulations in JAERI.

-
- [1] R.Kleiner, F.Steinmeyer, G.Kunkel, and P.Müller, *Phys.Rev.Lett.* **68**, 2394(1992); Y. Matsuda, M. B. Gai-fullin, K. Kumagai, K. Kadowaki, and T. Mochiku, *Phys. Rev. Lett.* **75**, 4512 (1995).
 - [2] R.Kleiner, P.Müller, H.Kohlstedt, N.F.Pedersen, and S.Sakai, *Phys.Rev.* **B50**,3942(1994); R.Kleiner, *Phys. Rev.* **B50**,6919(1994).
 - [3] S.Sakai, P.Bodin, and N.F.Pedersen, *J. Appl. Phys.* **73** (5), 2411(1993); S.Sakai, A.V.Ustinov, H.Kohlstedt, A.Petraglia, and N.F.Pedersen, *Phys. Rev.* **B50**, 12905 (1994); S.Sakai, A.V.Ustinov, N.Thyssen, and H.Kohlstedt, *Phys. Rev.* **B58**, 5777 (1998).
 - [4] A.V.Ustinov and H.Kohlstedt, *Phys. Rev.* **B54**,6111(1996).
 - [5] N.Gronbech-Jensen, J.A.Blackburn, and M.R.Samuelsen, *Phys. Rev.* **B53**, 12364(1996).
 - [6] V.M.Krasnov and D.Winkler, *Phys. Rev.* **B56**, 9106(1997).
 - [7] A.V.Ustinov and S.Sakai, *Appl. Phys. Lett.* **73**, 686(1998).
 - [8] A.Barone, and G.Paterno, *Physics and Applications of the Josephson Effect* (Wiley, New York, 1982).
 - [9] A.A.Abrikosov *Fundamentals of the Theory of Metals* (North-Holland, 1988).
 - [10] Y.M.Zhang, D.Winkler, P.A.Nilsson, and T.Claeson, *Phys. Rev.* **B51**,8684(1995). This is a recent experimental result for fluxon dynamics in SLJJ's. Many references therein.
 - [11] See the above ref.(1)~(6), and many references therein.
 - [12] S.N.Artemenko and S.V.Remizov, *JETP Lett.*,66,854(1997).
 - [13] M.Tachiki, T.Koyama, and Sakahashi, in *Coherence in High Temperature Superconductors*, edited by G.Deutcher and A.Revcolevshi (World Scientific Singapore, 1996), p.371.
 - [14] T.Koyama and M.Tachiki, *Phys. Rev.* **B54**,16183(1996); M.Machida, T.Koyama, and M.Tachiki *PhysicaC*

- 300**,55(1998).
- [15] L.N.Bulaevskii, M.Zamora, D.Baeriswyl, H.Beck, and J.R.Clem, *Phys. Rev.***B50**,12831 (1994); L.N.Bulaevskii, D.Dominguez, M.P.Maley, A.R.Bishop, and B.I.Ivlev, *Phys. Rev.***53**,14601 (1996).
 - [16] S.E.Shafranjuk, M.Tachiki, and T.Yamashita, *Phys. Rev.***57**, 13765(1998).
 - [17] A.V.Ustinov, H.Kohlstedt, and P.Henne, *Phys. Rev. Lett.* **77**, 3617(1996).
 - [18] G.Hechtfisher, R.Kleiner, A.V.Ustinov, and P.Muller, *Phys. Rev. Lett.* **79** , 1365(1997).
 - [19] G.Hechtfisher, R.Kleiner, A.V.Ustinov, and P.Muller, *Appl. Supercon.* **5**, 303(1998).